



Beyond DGLAP improved saturation model

G. R. Boroun^a

Department of Physics, Razi University, Kermanshah 67149, Iran

Received: 9 September 2022 / Accepted: 3 January 2023 / Published online: 19 January 2023
 © The Author(s) 2023

Abstract We present a modification of the DGLAP improved saturation model with respect to the nonlinear correction (NLC). The GLR-MQ improved saturation model is considered by employing the parametrization of proton structure function due to the Laplace transforms method, which preserves its behavior success in the low and high Q^2 regions. We show that the geometric scaling holds for the GLR-MQ improved model in a wide kinematic region rQ_s . These results are comparable with other models in a wide kinematic region rQ_s . The behavior of the dipole cross sections, with respect to the GLR-MQ improved saturation model, are comparable with the Color Glass Condensate (CGC) model. The model describes the dipole cross sections in the inclusive and diffractive processes. We also compare the nonlinear corrections to the impact-parameter dependent saturation (IP-Sat) model with the impact-parameter dependent color glass condensate (b-CGC) dipole model. Finally, we consider the linear and nonlinear corrections to the IP Non-Sat model. These results provide a benchmark for further investigation of QCD at small x in future experiments such as the Large Hadron Collider and Future Circular Collider projects.

1 Introduction

The color dipole picture (CDP) [1,2] has been introduced to study a wide variety of small x inclusive and diffractive processes at HERA. The dipole approach, at small values of Bjorken x , gives a clear interpretation of the high-energy interactions. This regime of QCD is characterized by high gluon densities because the proton structure is dominated by dense gluon systems [3–5] and predicts that the small x gluons in a hadron wavefunction should form a Color Glass Condensate [6–8]. The gluon saturation effects are observable at very small x values and characterized by a hard saturation

momentum $Q_s(x)$. The saturation scale is a border between dense and dilute gluonic systems as

$$xg(x, Q_s^2) \frac{\alpha_s(Q_s^2)}{Q_s^2} \simeq \pi R^2, \quad (1)$$

where $xg(x, Q^2)$ is the gluon distribution function and πR^2 is the target area where R is the correlation radius between two interacting gluons. Indeed the parameter R controls the strength of the nonlinearity. The saturation scale rises with decreasing x and at small enough x , $Q_s \gg \Lambda_{\text{QCD}}$ where Λ_{QCD} is the QCD cut-off parameter at each heavy quark mass threshold (i.e., $\Lambda_{\text{QCD}}^{n_f}$).

Since nonlinear dynamics are known to become sizable only at small- x , so the nonlinear contribution to the Dokshitzer–Gribov–Lipatov–Altarelli–Parisi (DGLAP) evolution [9–11] leads to an equation of the form

$$\frac{\partial^2 xg(x, Q^2)}{\partial \ln(1/x) \partial \ln Q^2} = \bar{\alpha}_s xg(x, Q^2) - \frac{9}{16} \bar{\alpha}_s^2 \pi^2 \frac{[xg(x, Q^2)]^2}{R^2 Q^2}, \quad (2)$$

where $\bar{\alpha}_s \equiv \alpha_s C_A / \pi$ and the value of R is order of the proton radius ($R \simeq 5 \text{ GeV}^{-1}$), if the gluons are distributed through the whole of proton, or much smaller ($R \simeq 2 \text{ GeV}^{-1}$) if gluons are concentrated in hot spot within the proton. This was a vast subject initiated by Gribov, Levin, Ryskin, Mueller and Qiu (GLR-MQ) [12,13], as the second nonlinear term in (2) is responsible for gluon recombination. This term arises from perturbative QCD diagrams which couple four gluons to two gluons. So that two gluon ladders recombine into a single gluon ladder. It leads to saturation of the gluon density at low Q^2 with decreasing x . A closer examination of the small x scattering is resummation powers of $\alpha_s \ln(1/x)$ where leads to the k_T -factorization form [14–16]. In the k_T -factorization approach the large logarithms $\ln(1/x)$ are relevant for the unintegrated gluon density in a nonlinear equation. Solution

^a e-mail: boroun@razi.ac.ir (corresponding author)

of this equation develops a saturation scale where tame the gluon density behavior at low values of x and this is an intrinsic characteristic of a dense gluon system [17].

The main goal of this paper is to consider the nonlinear corrections to the DGLAP improved saturation model. In fact, the DGLAP improved saturation model will be modified to the GLR-MQ improved saturation model. This is based on the nonlinear evolution of the gluon density at small values of x . These results will be compared with the nonlinear saturation dynamics which is explicitly incorporated into the CGC model. One of the well-known impact-parameter dependent saturation models is the IP-Sat model [18–22]. This is a simple dipole model that incorporates the physics of saturation and all known properties of the gluon saturation. In this case the saturation boundary is approached via the DGLAP evolution, that is, by the eikonalization of the gluon distribution, which effectively represents higher twist contributions. The b-CGC and the IP-Sat models are easily generalized from DIS off protons to DIS off nuclei [23,24].

This paper is organized as follows. In Sect. 2, we introduce the color dipole model for calculating the dipole cross sections in the GBW, the DGLAP improved saturation, the b-CGC dipole, the IP-Sat models and also the exclusive diffractive processes. In Sect. 3, we present the GLR-MQ improved saturation model to consider the color dipole cross section at low values of x . Then in Sect. 4, we present a detailed numerical analysis and our main results. We summarize our main results in Sect. 5.

2 Dipole cross section

Dipole representation provides a convenient description of DIS at small x . There, the scattering between the virtual photon γ^* and the proton is seen as the color dipole where the transverse dipole size r and the longitudinal momentum fraction z with respect to the photon momentum are defined. The amplitude for the complete process is simply the production of these subprocess amplitudes, as the DIS cross section is factorized into a light-cone wave function and a dipole cross section. Using the optical theorem, this leads to the following expression for the γ^*p cross-sections

$$\sigma_{L,T}^{\gamma^*p}(x, Q^2) = \int dz d^2\mathbf{r} |\Psi_{L,T}(\mathbf{r}, z, Q^2)|^2 \sigma_{\text{dip}}(x, \mathbf{r}), \quad (3)$$

where subscripts L and T referring to the transverse and longitudinal polarization state of the exchanged boson. Here $\Psi_{L,T}$ are the appropriate spin averaged light-cone wave functions of the photon and $\sigma_{\text{dip}}(x, r)$ is the dipole cross-section which related to the imaginary part of the $(q\bar{q})p$ forward scattering amplitude. The variable z , with $0 \leq z \leq 1$, characterizes the distribution of the momenta between quark and antiquark. The square of the photon wave function describes

the probability for the occurrence of a $(q\bar{q})$ fluctuation of transverse size with respect to the photon polarization [1–3]. The dipole hadron cross section σ_{dip} contains all information about the target and the strong interaction physics with

$$\sigma_{\text{dip}}(x, r) = \int d^2b \frac{d\sigma_{\text{dip}}}{d^2b}, \quad (4)$$

where b is a particular impact parameter (IP) as

$$\frac{d\sigma_{\text{dip}}}{d^2b} = 2(1 - \text{Re } S(b)), \quad (5)$$

and $S(b)$ is the S-matrix element of the elastic scattering. The cross section at a given impact parameter b is proportional to the dipole area, the strong coupling, the number of gluons in the cloud and the shape function by the following form [18–20]

$$\frac{d\sigma_{\text{dip}}}{d^2b} = 2 \left[1 - \exp \left(- \frac{\pi^2 r^2 \alpha_s(\mu^2) x g(x, \mu^2) T(b)}{2N_c} \right) \right], \quad (6)$$

where the hard scale is assumed to have the form

$$\mu^2 = C/r^2 + \mu_0^2, \quad (7)$$

and the parameters C and μ_0^2 are obtained from the fit to the DIS data [1,2]. For multi Pomeron exchange, the eikonalised dipole scattering amplitude of Eq. (6) can be expanded as

$$N(x, r, b) = \sum_{n=1}^{\infty} \frac{(-1)^{n+1}}{n!} \left[\frac{\pi^2}{2N_c} r^2 \alpha_s(\mu^2) x g(x, \mu^2) T(b) \right]^n,$$

where $d\sigma_{\text{dip}}/d^2b = 2N(x, r, b)$ and the n -th term in the expansion corresponds to n -Pomeron exchange [18–20]. Equation (6) is known as the Glauber–Mueller dipole cross section [25] and can also be obtained within the McLerran–Venugopalan model [26]. The exponential form of the function $T(b)$ is determined from the fit to the data as

$$T(b) = \frac{1}{2\pi B_G} \exp(-b^2/2B_G), \quad (8)$$

where the parameter B_G was found [18–20] to be 4.25 GeV^{-2} .

In the original Golec-Biernat–Wüsthoff (GBW) model [1, 2], the dipole cross section was proposed to have the eikonal-like form

$$\sigma_{\text{dip}}(x, r) = \sigma_0(1 - e^{-r^2 Q_s^2/4}), \quad (9)$$

where $Q_s(x)$ plays the role of the saturation momentum, parametrized as $Q_s^2(x) = Q_0^2(x/x_0)^{-\lambda}$. Parameters Q_0 and x_0 set dimension and absolute value of the saturation scale and exponent λ governs x behavior of Q_s^2 . This model was updated in [3,27,28] to improve the large Q^2 description of the proton structure function by a modification of the small r behavior of the dipole cross section to include the DGLAP evolved gluon distribution. Since the energy dependence in large Q^2 region is mainly due to the behavior of the dipole cross section at small dipole size r , therefore authors in

Refs. [3,27,28] investigated the DGLAP evolution for small dipoles. Bartels–Golec-Bienat-Kowalski (BGBK) improved the dipole cross section by adding the collinear DGLAP effects. Indeed the BGBK model is the implementation of QCD evolution in the dipole cross section which depends on the gluon distribution. The following modification of the DGLAP improved saturation model [1,2] proposed for the dipole cross section as

$$\sigma_{\text{dip}} = \sigma_0 \left\{ 1 - \exp \left(- \frac{\pi^2 r^2 \alpha_s(\mu^2) x g(x, \mu^2)}{3\sigma_0} \right) \right\}. \quad (10)$$

Indeed BGBK model is successful in describing dipole cross section at large values of r as the two models (GBW and BGBK) overlap in this region but they differ in the small r region where the running of the gluon distribution starts to play a significant role. Indeed the DGLAP improved model of σ_{dip} significantly improves agreement at large values of Q^2 without affecting the physics of saturation responsible for transition to small Q^2 . As expected, geometrical scaling is true for the DGLAP improved model curve for the scaling variable $r Q_s \geq 1$ and for the GBW model curve for the whole region [1,2].

The saturated version of the dipole model may in principle be derived from the Color Glass Condensate effective theory for QCD according to Eq. (6) where at small r this expression (i.e., Eq. (6)) becomes

$$\frac{d\sigma_{\text{dip}}}{d^2b} = \frac{\pi^2 r^2 \alpha_s(\mu^2) x g(x, \mu^2) T(b)}{N_c}. \quad (11)$$

Equation (6) is referred to as the IP-Sat model, while Eq. (11) is referred to as the IP Non-Sat model. The BGBK and CGC models considered only the dipole cross section integrated over the impact parameter b [29]. The BGBK model was modified to include the impact parameter dependence as denoted by the IP-Sat model and the CGC model was also modified to include the impact parameter dependence as denoted by the b-CGC model. The dipole cross section can be calculated in the CGC approach from the relation

$$\sigma_{\text{dip}}(x, r) = \sigma_0 \mathcal{N}(x, r), \quad (12)$$

where $\sigma_0 = 2\pi R_p^2$ and

$$\mathcal{N}(x, r) = \begin{cases} \mathcal{N}_0 \left(\frac{r Q_s}{2} \right)^{2(\gamma_s + (1/k\lambda Y) \ln(2/r Q_s))} & r Q_s \leq 2 \\ 1 - e^{-A \ln^2(B r Q_s)} & r Q_s > 2, \end{cases} \quad (13)$$

where $Y = \ln(1/x)$ and $k = \chi''(\gamma_s)/\chi'(\gamma_s)$ where χ is the LO BFKL [30–32] characteristic function. The scattering amplitude $\mathcal{N}(x, r)$ can vary between zero and one, where $\mathcal{N} = 1$ is the unitarity limit. To introduce the impact parameter dependence into the CGC model, the b-CGC model for the dipole cross section is defined by the following form [29]

$$\frac{d\sigma_{\text{dip}}}{d^2b} = 2\mathcal{N}(x, r, b) \quad (14)$$

where the impact parameter dependence of the saturation scale Q_s was introduced by

$$Q_s \equiv Q_s(x, b) = \left(\frac{x_0}{x} \right)^{\lambda/2} \left[\exp \left(- \frac{b^2}{2B_{CGC}} \right) \right]^{1/2\gamma_s}, \quad (15)$$

where the parameter B_{CGC} , instead of σ_0 in the CGC dipole model, is a free parameter and is determined by other reactions, namely the t distribution of the exclusive diffractive processes at HERA. The parameters were fixed by a combination of theoretical constraints [21,22] and a fit to DIS data.

Another one of the main advantages of dipole models is the description of the diffractive process [3,33,34]. The cross section for the diffractive $q\bar{q}$ production reads [14–16]

$$\frac{d\sigma_{L,T}^D}{dt} \Big|_{t=0} = \int dz d^2\mathbf{r} |\Psi_{L,T}(\mathbf{r}, z)|^2 \sigma_{\text{dip}}^2(x, \mathbf{r}), \quad (16)$$

where $t = \Delta^2$, and Δ is the four-momentum transferred into the diffractive system from the proton. In Eq. (16), the generalised optical theorem is applied in the framework of the dipole picture. At small values of the diffractive mass $M^2 \sim Q^2$ the elastic scattering of the $q\bar{q}$ pair dominates, while at larger values of the mass $M^2 \gg Q^2$, the $q\bar{q}g$ contribution dominates (due to gluon production in the final diffractive state). The treatment of the $q\bar{q}g$ component goes beyond the saturation model since this is not present in the inclusive analysis [3,33,34]. This component was computed in the two gluon exchange approximation with an additional assumption of strong ordering of transverse momenta of the $q\bar{q}$ pair and the gluon. In the transverse coordinate representation, the $q\bar{q}g$ system is treated as a color octet dipole $8\bar{8}$ where the coupling of two t -channel gluons is relative by a weight factor $C_A/C_F = 2N_C^2/(N_C^2 - 1)$ with $C_A = N_c = 3$ and $C_F = \frac{N_C^2 - 1}{N_C} = \frac{4}{3}$ where N_C is the number of colors. Thus, the color dipole cross section for exchange of a two gluon system for octet dipole reads [3,33,34]

$$\sigma_{\text{dip}} = \sigma_0 \left\{ 1 - \exp \left(- \frac{C_A}{C_F} \frac{\pi^2 r^2 \alpha_s(\mu^2) x g(x, \mu^2)}{3\sigma_0} \right) \right\}. \quad (17)$$

In the next section, we consider the color dipole cross sections due to the behavior of the linear and nonlinear gluon density and compare with the other models. The linear gluon densities are obtained with respect to the Laplace transform technique by employing the parametrization of proton structure function, then applied the GLR-MQ evolution equation for the nonlinear gluon densities. Some approximated analytical solutions in the color dipole model have been reported in recent years [35,36] with considerable phenomenological success due to a parametrization of the deep inelastic structure function for electromagnetic scattering with protons.

3 GLR-MQ improved saturation model

We will present an approach to the description of the color dipole cross section at small x , alternative to that based on the DGLAP improved saturation model. From a more theoretical viewpoint it is known that in the low x , low Q^2 region gluon recombination effects are not negligible and reduce the growth of the gluon parton distribution function. The GLR-MQ equation for the gluon density, where an extra non-linear term, quadratic in the gluon density, was added to the linear DGLAP evolution equation by the following form

$$\frac{\partial xg(x, \mu^2)}{\partial \ln \mu^2} = \frac{\partial xg(x, \mu^2)}{\partial \ln \mu^2}|_{\text{DGLAP}} - \frac{81\alpha_s^2}{16R^2\mu^2} \int_{\chi}^1 \frac{dy}{y} [yg(y, \mu^2)]^2, \quad (18)$$

where $\chi = \frac{x}{x_0}$ and x_0 is the boundary condition that the gluon distribution (i.e., $G(x, \mu^2) = xg(x, \mu^2)$) joints smoothly onto the linear region. We note that at $x \geq x_0 (= 10^{-2})$ the non-linear corrections are negligible. The nonlinear shadowing term, $\propto -[g]^2$, arises from perturbative QCD diagrams. In this regime the gluons in the proton form a dense system with mutual interaction and recombination which also leads to the saturation of the total cross section. Other early works on this topic can be found in [37–40]. In what follows, the hard scale is assumed to have the form $\mu^2 = C/r^2 + \mu_0^2$ as for light quarks the gluon distribution is evaluated at $x = x_{BJ} = \mu^2/(\mu^2 + W^2)$ and for the charm quark the gluon structure function is evaluated at

$$x = (\mu^2 + 4m_c^2)/(\mu^2 + W^2), \quad (19)$$

where m_c is the charm quark mass and W refers to the photon-proton center-of-mass energy. The non-linear equation (i.e., Eq. (18)) shows that the strong rise that is corresponding to the linear QCD evolution equations at small- x and Q^2 can be tamed by screening effects. The first iteration of Eq. 18 reads

$$dG(x, \mu^2)|_{\text{NLC}} = dG(x, \mu^2)|_{\text{DGLAP}} - \frac{81\alpha_s^2}{16R^2\mu^2} d\ln \mu^2 \times \int_{\chi}^1 \frac{dy}{y} [G(y, \mu^2)]^2, \quad (20)$$

where the nonlinear correction to the gluon distribution function (i.e., $G^{\text{NLC}}(x, \mu^2)$) is obtained by the following form

$$G^{\text{NLC}}(x, \mu^2) = G^{\text{NLC}}(x, \mu_0^2) + [G(x, \mu^2) - G(x, \mu_0^2)] - \int_{\mu_0^2}^{\mu^2} \frac{81}{16} \frac{\alpha_s^2(\mu^2)}{R^2\mu^2} \int_x^{x_0} \frac{dz}{z} G^2\left(\frac{x}{z}, \mu^2\right) d\ln \mu^2. \quad (21)$$

Here $G(x, \mu^2)$ and $G(x, \mu_0^2)$ are the linear gluon distributions, and obtained from the parametrization F_2 using the

Laplace transform techniques [41–43], at μ^2 and μ_0^2 scales respectively. At the initial scale μ_0^2 , the low x behavior of the non-linear gluon distribution is assumed to be [44]

$$G^{\text{NLC}}(x, \mu_0^2) = G(x, \mu_0^2) \left\{ 1 + \frac{27\pi\alpha_s(\mu_0^2)}{16R^2\mu_0^2} \theta(x_0 - x) \right. \\ \left. \times [G(x, \mu_0^2) - G(x_0, \mu_0^2)]^{-1} \right\}. \quad (22)$$

Therefore the non-linear correction to the gluon distribution at μ^2 scale for $x < x_0$ reads

$$G^{\text{NLC}}(x, \mu^2) = G(x, \mu^2) + G(x, \mu_0^2) \left[\left\{ 1 + \frac{27\pi\alpha_s(\mu_0^2)}{16R^2\mu_0^2} \right. \right. \\ \left. \left. \times [G(x, \mu_0^2) - G(x_0, \mu_0^2)]^{-1} - 1 \right\} \right. \\ \left. - \int_{\mu_0^2}^{\mu^2} \frac{81}{16} \frac{\alpha_s^2(\mu^2)}{R^2\mu^2} \right. \\ \left. \int_x^{x_0} \frac{dz}{z} G^2\left(\frac{x}{z}, \mu^2\right) d\ln \mu^2 \right]. \quad (23)$$

The gluon distribution due to the non-linear corrections can be analytically solved at small x with respect to the linear gluon distribution behavior.

The linear gluon distributions (i.e., $G(x, \mu^2)$ and $G(x, \mu_0^2)$) in Eq. (23) are defined with respect to the most parametrization suggested in Refs. [41–43]. The authors in Ref. [41] have an expression for the asymptotic part of F_2 (no-valence) as

$$F_2 \propto \ln^2(1/x) \quad (24)$$

for $x \leq 0.09$. In Refs. [42,43], the authors obtained two quadratic expressions in $\ln^2(1/x)$ using second-order linear differential equation as well as Laplace transforms for the leading-order (LO) gluon distribution function, respectively. In the first method in Refs. [42,43], the LO DGLAP equation for the evolution of the proton structure function $F_2(x, Q^2)$ is rearranged into an inhomogeneous second-order differential equation by the following form

$$x^2 \frac{\partial^2}{\partial x^2} G(x, Q^2) - 2x \frac{\partial}{\partial x} G(x, Q^2) + 4G(x, Q^2) \\ = -\frac{4\pi}{\alpha_s} \frac{9}{20} x^4 \frac{\partial^4}{\partial x^3 \partial \ln Q^2} \frac{F_2(x, Q^2)}{x} + \frac{12}{5} x \frac{\partial}{\partial x} F_2(x, Q^2) \\ - 3x^2 \frac{\partial^2}{\partial x^2} F_2(x, Q^2) - \frac{9}{5} x^3 \frac{\partial^3}{\partial x^3} F_2(x, Q^2) \\ + \frac{12}{5} x^4 \frac{\partial^3}{\partial x^3} \int_x^1 \frac{\partial}{\partial x} F_2(z, Q^2) \ln \frac{z}{z-x} dz. \quad (25)$$

Equation (25), with the new variable $v = \ln(1/x)$ becomes a linear 2^{nd} order inhomogeneous equation, as

$$\left(\frac{\partial^2}{\partial v^2} + 3 \frac{\partial}{\partial v} + 4 \right) \widehat{G}(v, Q^2) = \widehat{\mathcal{G}}_4(v, Q^2) \quad (26)$$

and the definition $\widehat{G}(v, Q^2) = G(e^{-v}, Q^2)$. In Refs. [42, 43], the authors have found the parametrization of the gluon distribution $\widehat{G}_4(v, Q^2)$ which is calculated as a second degree polynomial in v whose coefficients are quadratic polynomials in $\ln(Q^2)$ for $x \leq 0.09$ as

$$\widehat{G}_4(v, Q^2) = \alpha(Q^2) + \beta(Q^2)v + \gamma(Q^2)v^2, \quad (27)$$

Therefore

$$\widehat{G}(v, Q^2) = \frac{2}{\sqrt{7}} \int_0^v e^{-\frac{3}{2}(v-v')} \sin\left(\frac{\sqrt{7}}{2}(v-v')\right) \widehat{G}_4(v', Q^2) dv',$$

where the gluon distribution in x -space reads as a simple quadratic polynomial in $\ln(1/x)$ with quadratic polynomial coefficients in $\ln(Q^2)$ by the following form

$$\begin{aligned} G(x, Q^2) = & -0.459 - 0.143 \ln Q^2 - 0.0155 \ln^2 Q^2 \\ & + \left[0.231 + 0.00971 \ln Q^2 - 0.0147 \ln^2 Q^2 \right] \ln(1/x) \\ & + \left[0.0836 + 0.06328 \ln Q^2 + 0.0112 \ln^2 Q^2 \right] \ln^2(1/x). \end{aligned} \quad (28)$$

In the second method, the authors [42, 43] have suggested a new parametrization based on Laplace transforms. The DGLAP evolution is written as follows

$$\int_0^v \widehat{G}(w, Q^2) \widehat{h}(v-w) dw = \widehat{f}(v, Q^2), \quad (29)$$

where $w = \ln(1/z)$ and

$$\widehat{f}(v, Q^2) = \frac{3}{4} \frac{4\pi}{\alpha_s} \mathcal{F}_2(e^{-v}, Q^2). \quad (30)$$

The function $\widehat{h}(v)$ in Eq. (29) is

$$\widehat{h}(v) = e^{-v} \widehat{P}_{gq}(v), \quad (31)$$

where P_{gq} is the gluon-quark splitting function. The function $\mathcal{F}_2(x, Q^2)$ in Eq. (30) is sum of the proton structure function F_2 -dependent terms in the DGLAP evolution equation by

$$\begin{aligned} \mathcal{F}_2(x, Q^2) = & \frac{\partial F_2(x, Q^2)}{\partial \ln Q^2} - \frac{\alpha_s}{4\pi} \left\{ \frac{16}{3} \int_x^1 \frac{\partial F_2(z, Q^2)}{\partial z} \right. \\ & \times \ln \frac{z}{z-x} dz - \frac{4}{3} \int_x^1 \frac{\partial F_2(z, Q^2)}{\partial z} \left(\frac{x^2}{z^2} + \frac{2x}{z} \right) dz \left. \right\}. \end{aligned} \quad (32)$$

By making a Laplace transform in v , we can factor Eq. (29), since the Laplace transform of a convolution is the product of the Laplace transform of the factors, so that

$$\mathcal{L} \left\{ \int_0^v \widehat{G}(w, Q^2) \widehat{h}(v-w) dw; s \right\} = \widehat{g}(s, Q^2) \times \widehat{h}(s) \quad (33)$$

Solving Eq. (29) for g in s -space, we have

$$\widehat{g}(s, Q^2) = \widehat{h}^{-1}(s) \widehat{f}(s, Q^2). \quad (34)$$

Thus, inverting the Laplace transform of the factors, then the gluon distribution is defined by

$$\widehat{G}(v, Q^2) = \mathcal{L}^{-1} \left[\widehat{h}^{-1}(s) \widehat{f}(s, Q^2); v \right]. \quad (35)$$

Therefore, the gluon distribution in x -space reads

$$\begin{aligned} G(x, Q^2) = & \frac{9}{20} \frac{4\pi}{\alpha_s} \left\{ 3 \mathcal{F}_2^{\gamma p}(x, Q^2) - x \frac{\partial}{\partial x} \mathcal{F}_2^{\gamma p}(x, Q^2) \right. \\ & - \int_x^1 \mathcal{F}_2^{\gamma p}(z, Q^2) \left(\frac{x}{z} \right)^{3/2} \\ & \left[\frac{6}{\sqrt{7}} \sin \left(\frac{\sqrt{7}}{2} \ln \left(\frac{z}{x} \right) \right) \right. \\ & \left. \left. + 2 \cos \left(\frac{\sqrt{7}}{2} \ln \left(\frac{z}{x} \right) \right) \right] \right\}, \end{aligned} \quad (36)$$

for $0 < x \leq 0.06$. The standard representation for QCD coupling in LO approximation is defined by

$$\alpha_s^{\text{LO}}(t) = \frac{4\pi}{\beta_0 t}, \quad (37)$$

where β_0 is the one loop correction to the QCD β -function and $t = \ln \frac{Q^2}{\Lambda^2}$, Λ is the QCD cut-off parameter with $\alpha_s(M_z^2) = 0.118$.

The $\ln^2(1/x)$ behavior of the DIS proton structure function (i.e., Eq. (24)) at small values of x is compatible with saturation of the Froissart bound at each value of Q^2 . The authors, in Ref. [41], have shown that this behavior may be the signal for the saturation or gluon recombination processes at high parton densities. The gluon distribution in Eqs. (26–36), according to the results in Refs. [42, 43], is determined from the DGLAP evolution equation for the proton structure function. Thus in Eq. (20), the nonlinear corrections to the gluon behavior at low x and Q^2 values are considered, where it is compatible with $\ln^2(1/x)$ behavior of parton densities at very small x in the QCD evolution framework.

Now, we can estimate the non-linear corrections to the gluon distribution (i.e., Eq. (23)) due to the linear gluon distributions (i.e., Eqs. (28) and (36)) for small x and we will use the non-linear corrections to the dipole cross sections, and in the next section, the accuracy of the results will be discussed in comparison with the CGC model.

4 Results

The linear and nonlinear methods are presented based on the solutions of the DGLAP and GLR-MQ evolution equations at the leading-order accuracy in perturbative QCD, respectively. The dipole cross-sections (Eqs. 6, 10, 11 and 17) require the gluon density $G(x, \mu^2)$ for all scales μ^2 . These gluon distributions [42, 43] are obtained directly in terms of the parameterization of the structure function $F_2(x, \mu^2)$ and its

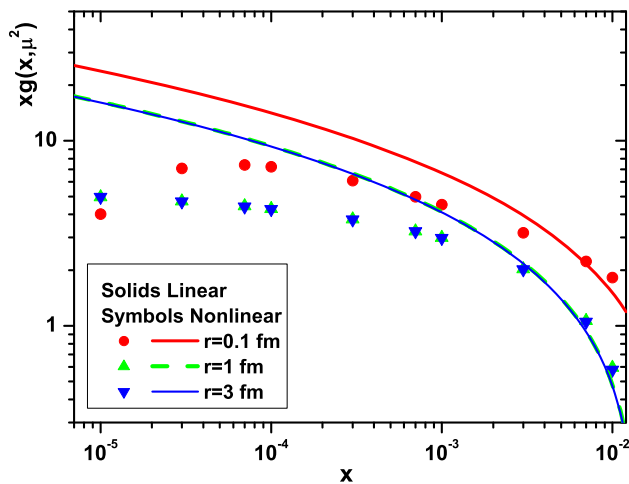


Fig. 1 The linear (Eqs. (28) and (36)) and nonlinear (Eq. (23)) gluon distribution functions for various dipole sizes

derivative. The resulting linear and nonlinear gluon distribution functions for various dipole sizes for $x \leq 10^{-2}$ are shown in Fig. 1. The dipole size determines the evolution scale μ^2 .

In this figure, we plot the r dependence of the nonlinear corrections to the gluon distribution for $R = 2 \text{ GeV}^{-1}$. Nonlinear corrections play an important role on gluon distribution as x and μ^2 decrease. A depletion occurs at $x < 10^{-2}$ where these results show that the nonlinear behavior of the gluon distribution function is tamed. This taming behavior of nonlinear gluon distribution function toward low x at low μ^2 values becomes significant when considering the color dipole cross section at the hot spot point (i.e., $R = 2 \text{ GeV}^{-1}$). We have calculated the linear and nonlinear corrections to the ratio $\sigma_{\text{dip}}/\sigma_0$ in a wide range of the dipole size at the LO approximation. Results of calculations and comparison with the GBW [1,2] and CGC [6–8] models for $x = 10^{-4}$ are presented in Fig. 2. The linear corrections to the ratio of color dipole cross sections at LO approximation are comparable with the GBW model at low and high r values. The nonlinear corrections to the ratio of color dipole cross sections are comparable with the GBW model for $r \lesssim 10^{-2}$ and $r \gtrsim 10^0$ and also are comparable with the CGC model for $10^{-2} \lesssim r \leq 10^0$. Indeed the nonlinear corrections tame the behavior of the dipole cross section at $r \gtrsim 10^{-1}$. The effective parameters in the GBW model have been extracted from a fit of the HERA data as, $\lambda = 0.288$, $x_0 = 3.04 \times 10^{-4}$, $C = 0.38$ and $\mu_0^2 = 1.73$ [1,2]. Parameters of the CGC dipole model fixed at the LO BFKL according to the original CGC fit [6–8] with respect to the values $\gamma_s = 0.63$, $k = 9.9$, $N_0 = 0.7$, $\lambda = 0.177$ and $x_0 = 2.70 \times 10^{-7}$ [29]. The dipole cross sections are evaluated according to the four active flavors, which take into account charm quark mass. The quark mass, in the CGC model, was taken to be 1.4 GeV although in our calculations it is 1.29 GeV [45].

An important property of the saturation formalism is the geometric scaling phenomenon, which means that the scat-

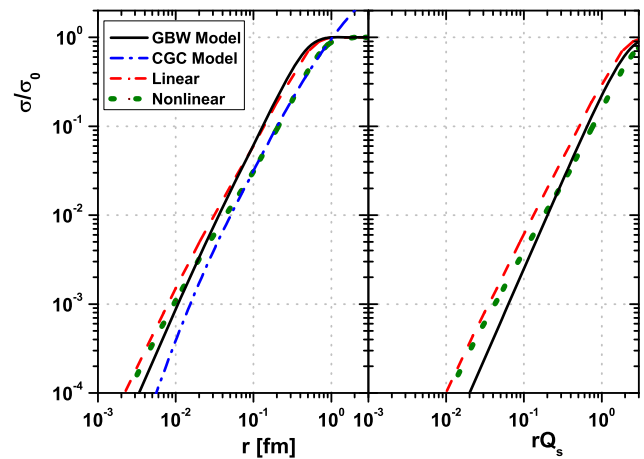


Fig. 2 Left: the extracted linear (dashed curve) and nonlinear (dot curve) ratio $\sigma_{\text{dip}}/\sigma_0$ (Eq. (10)) as a function r for $x = 10^{-4}$ compared with the GBW model (Eq. (9)) (solid curve) and CGC model (Eq. (13)) (dashed-dot curve, CGC plotted due to Eq. (13) for $rQ_s \leq 2$ and also the parameters are defined from Ref. [29]). Right: the same as left as a function rQ_s

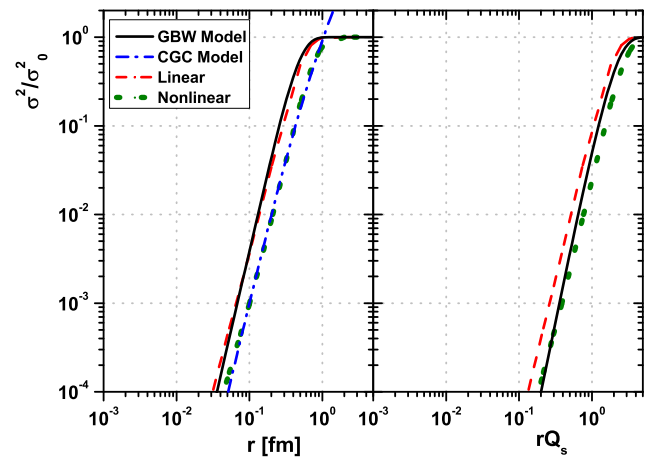


Fig. 3 The same as Fig. 2 in the simplest case of the $q\bar{q}$ system for the ratio $\sigma_{\text{dip}}^2/\sigma_0^2$ (Eq. (16))

tering amplitude and corresponding cross sections can scale on the dimensionless scale rQ_s . A particular interests present the linear and nonlinear ratio $\sigma_{\text{dip}}/\sigma_0$ defined by the scaling variable rQ_s . In Fig. 2 (right hand), we observe that the nonlinear corrections to the ratio $\sigma_{\text{dip}}(rQ_s(x))/\sigma_0$ merge into the GBW curve for $rQ_s \gtrsim 10^{-1}$. The results of the GLR-MQ improved saturation model due to the parametrization of the proton structure function have become a function of a single variable, rQ_s , for almost all values of r at LO approximation.

The diffractive final state [3,33,34] is built starting from a $q\bar{q}$ pair in the color singlet state as the diffractive $\gamma^* p \rightarrow q\bar{q} p'$ cross section is proportional to $\sigma^2(x, r)$ by Eq. (16). We have calculated the ratio $\sigma_{\text{dip}}^2/\sigma_0^2$ for the diffractive $q\bar{q}$ production into r and rQ_s respectively and compared the ratio with the GBW and CGC models in Fig. 3. The linear corrections to the ratio $\sigma_{\text{dip}}^2/\sigma_0^2$ are comparable with the GBW model in a wide

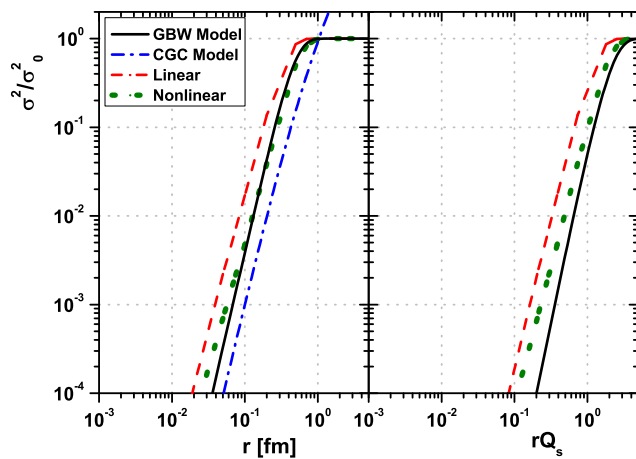


Fig. 4 The same as Fig. 3 for the $q\bar{q}g$ component of the diffractive system in the ratio $\sigma_{\text{dip}}^2/\sigma_0^2$ (Eq. (17))

range of r although the nonlinear corrections are comparable with the CGC model for $r < 1$ and with the GBW model for $r \geq 1$. In Fig. 3 (left hand), the geometrical scaling of the nonlinear corrections to the ratio $\sigma_{\text{dip}}^2/\sigma_0^2$ is visible in comparison with the linear curve. The nonlinear curve merges into one solid line in the right plot where the dipole cross section is plotted as a function of the scaling variable rQ_s . This is a reflection of geometric scaling in the nonlinear corrections in comparison with the GBW model for the diffractive $q\bar{q}$ production.

In addition to the contributions of the $q\bar{q}$ states, it is important to include the contributions of the $q\bar{q}g$ final states of the diffractive processes in the nonlinear corrections to the ratio $\sigma_{\text{dip}}^2/\sigma_0^2$. In Fig. 4 the ratio of the dipole cross sections are determined by the $q\bar{q}g$ component and are compared with the GBW and CGC models. The linear and nonlinear ratio of the dipole cross sections, in comparison with the results in Fig. 3, are deviated from the GBW and CGC models respectively. The reason for this deviation is because the $q\bar{q}g$ component, interacting with the proton with the same dipole cross section as the $q\bar{q}$ system, goes beyond the saturation model [33,34]. Indeed, in Fig. 4, the linear and nonlinear cross sections are modified due to the weighted factor C_A/C_F although this component is not present in the inclusive analysis.

Now we consider the nonlinear corrections to the $q\bar{q}$ differential cross section $d\sigma_{\text{dip}}/d^2b$. In Fig. 5, the linear and nonlinear corrections to the impact parameter dependent dipole cross section due to the GLR-MQ equation are considered and compared with the b-CGC model for $x = 10^{-4}$. In this figure (i.e., Fig. 5) the linear corrections to the IP-Sat (i.e., b-Sat) model are comparable with the b-CGC model in a wide range of the impact parameter b for $r < 1$ fm and the nonlinear corrections to the IP-Sat model are comparable with the b-CGC model in a wide range of the impact parameter b for $r \geq 1$ fm. The optimum values for the b-CGC model parameters are the following [29]: $\gamma_s = 0.46$, $B_{\text{CGC}} = 7.5 \text{ GeV}^{-1}$,

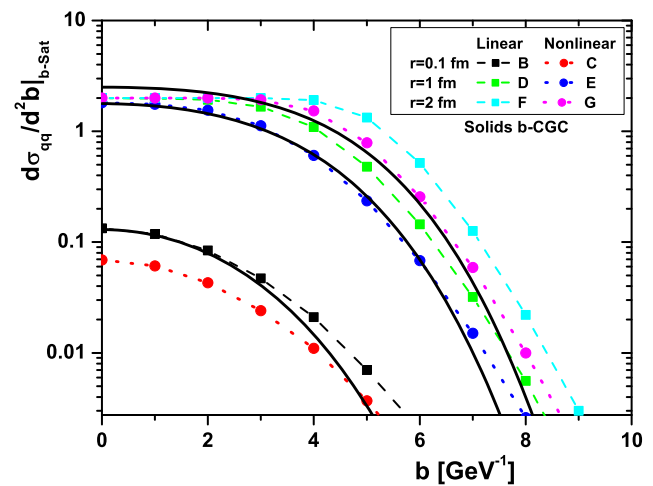


Fig. 5 The linear and nonlinear corrections to the impact parameter dependent dipole cross section versus the impact parameter b (Eq. (6)) compared with the b-CGC model (Eq. (14)) for the dipole sizes $r = 0.1, 1$ and 2 fm at $x = 10^{-4}$

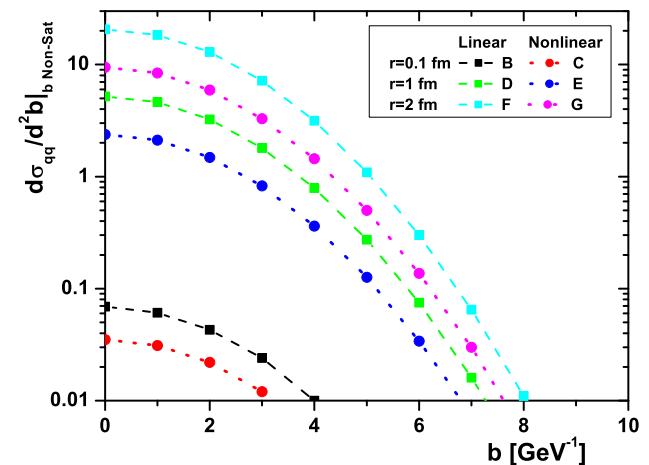


Fig. 6 The linear and nonlinear corrections to the IP Non-Sat (Eq. (11)) versus the impact parameter b for the dipole sizes $r = 0.1, 1$ and 2 fm at $x = 10^{-4}$

$N_0 = 0.558$, $x_0 = 1.84 \times 10^{-6}$ and $\lambda = 0.119$. In Fig. 5 we observe that the linear and nonlinear behavior of $d\sigma_{\text{dip}}/d^2b$ grows rapidly with r for small values of b , until those reach the saturation plateau, $d\sigma_{\text{dip}}/d^2b = 2$, which illustrates saturation in the Glauber–Mueller approach. Indeed, the GLR-MQ improved saturation model illustrates unitarity with an increase of r as b decreases.

At small r , the IP-Sat model (Eq. 6) becomes the IP Non-Sat model (Eq. 11) where the interaction between the dipole and the hadron is described by the exchange of one gluon. The linear and nonlinear behavior of $d\sigma_{\text{dip}}/d^2b$ in the IP Non-sat model are considered in Fig. 6. In this model, the behavior of the $d\sigma_{\text{dip}}/d^2b$ is directly dependent on the gluon distribution function. Saturation effects are not visible in this model as b decreases. However this behavior tamed due to the nonlinear corrections to the gluon density. For small dipole sizes the

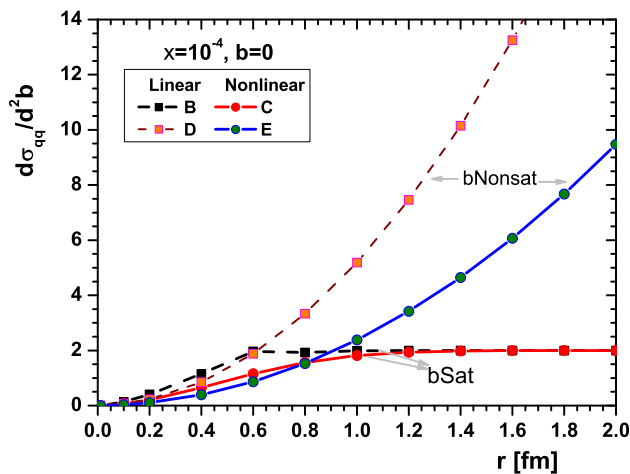


Fig. 7 Comparison of linear and nonlinear corrections to the $d\sigma_{\text{dip}}/d^2b$ for the IP-Sat (Eq. (6)) as well as IP Non-Sat (Eq. (11)) versus r for $x = 10^{-4}$ and $b = 0$

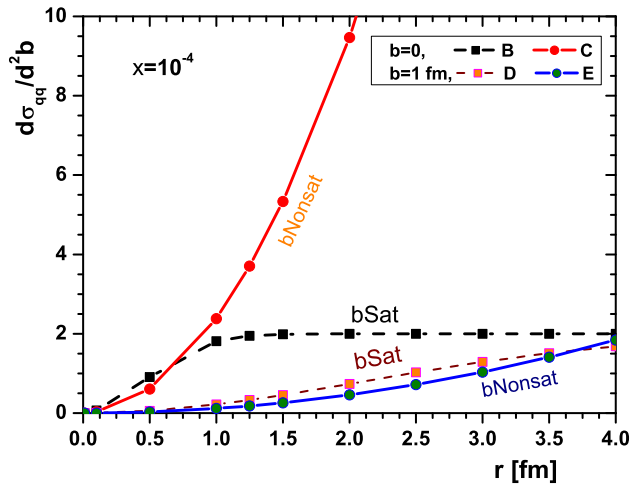


Fig. 8 Comparison of nonlinear corrections to the $d\sigma_{\text{dip}}/d^2b$ for the IP-Sat (Eq. (6)) as well as IP Non-Sat (Eq. (11)) versus r at $x = 10^{-4}$ for $b = 0$ and $b = 1$ fm, respectively

distributions are almost similar but they differ significantly as r becomes large.

A comparison of the resulting $d\sigma_{\text{dip}}/d^2b$ according to the linear as well as nonlinear behavior of the dipole cross section for $b = 0$ at $x = 10^{-4}$ presented in Fig. 7. The resulting dipole cross-sections in linear and nonlinear corrections are shown in Fig. 7. We observe that, in this figure, the nonlinear corrections suppress the behavior of the large dipoles in the IP Non-Sat model. Indeed, this behavior tamed at large r for $b = 0$ where with the increase r , μ decreases to the value of μ_0 . We also note that adding nonlinear corrections to the IP-Sat model decreases the dipole cross-section for $0.2 \text{ fm} < r < 1 \text{ fm}$ at $b = 0$. The linear and nonlinear corrections to the dipole cross section to the IP-Sat model reach the saturation plateau at $r > 1 \text{ fm}$.

It is interesting to increase the impact parameter from $b = 0$ to 1 fm for the nonlinear behavior of the dipole cross

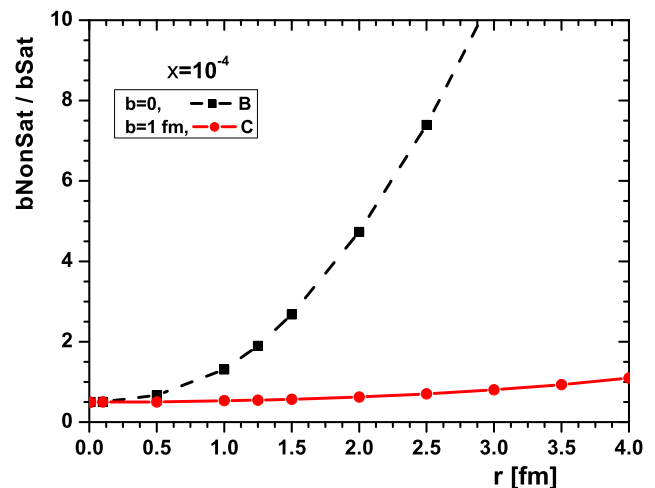


Fig. 9 The nonlinear corrections to the ratio IP Non-sat/IP-Sat (Eq. (11)/Eq. (6)) of the $d\sigma_{\text{dip}}/d^2b$ as a function r at $x = 10^{-4}$ for $b = 0$ and 1 fm , respectively

sections to the IP Non-Sat in Fig. 8. The proton dipole cross section at different impact parameters with and without nonlinear corrections are shown in Fig. 8 for the IP-Sat as well as IP Non-Sat versus r at $x = 10^{-4}$. The IP-Sat and IP Non-Sat dipole cross sections are very similar in the range $0 \leq r \leq 4 \text{ fm}$ for $b = 1 \text{ fm}$. Consequently, for large impact parameter sizes the distributions are almost similar but they differ significantly as b becomes small due to the nonlinear corrections. Indeed, the nonlinear corrections become stronger at larger impact parameters for the IP Non-Sat model [4]. In Fig. 9 we show the IP Non-Sat to IP-Sat cross-section ratios as a function of r for $x = 10^{-4}$. We depict the ratio as a function of r for $b = 0$ and 1 fm . Note that the ratio increases much faster as a function of r for $b = 0$ than for $b = 1 \text{ fm}$. We further note that at larger r , the ratio remains near almost unity for $b = 1 \text{ fm}$. The large difference between IP Non-Sat and IP-Sat comes from the decreases in the impact parameter values.

5 Conclusions

In this paper we proposed a modification of the saturation model which takes into account the GLR-MQ evolution of the gluon distribution. We have presented a certain theoretical model at LO approximation to describe the color dipole cross sections based on the Laplace transforms method at small values of x (the Bjorken variable x is fixed to be $x = 10^{-4}$). We have used a nonlinear correction to the dipole cross sections from a parametrization of the proton structure function with a rescaled variable m_c . The nonlinear corrections to the dipole cross sections in the description of inclusive and diffractive DIS at small x , according to the saturation scale and geomet-

ric scaling, are consistent with analytical saturation models in a wide range of r and rQ_s , respectively. We find that the ratio $\sigma_{\text{dip}}/\sigma_0$ due to the DGLAP improved saturation model is consistent with the GBW saturation model, although the nonlinear corrections to this ratio with respect to the GLR-MQ improved saturation model is consistent with the CGC saturation model especially in the range $0.05 < r \leq 1$. In the simplest case of the $q\bar{q}$ system for the ratio $\sigma_{\text{dip}}^2/\sigma_0^2$ in the diffractive processes, the linear and nonlinear corrections show good agreement with the GBW and CGC models in a wide range of r and rQ_s . The linear and nonlinear corrections to the ratio $\sigma_{\text{dip}}^2/\sigma_0^2$ in the diffractive processes due to the component $q\bar{q}g$ deviates from the GBW and CGC models, because the $q\bar{q}g$ system goes beyond the saturation models.

We developed nonlinear corrections to the impact parameter dependent dipole cross sections, $d\sigma_{\text{dip}}/d^2b$. The nonlinear corrections to the IP-Sat model are comparable with the b-CGC model in a wide range of the impact parameter b and the dipole size r . The linear and nonlinear corrections considered in the IP-Sat and IP Non-Sat models for the impact parameters $b = 0$ and $b = 1$ fm in the range $0 \leq r \leq 4$. The behavior of the nonlinear corrections to the IP Non-Sat model tamed in a wide range of r . This behavior for the IP-Sat model shows that the dipole cross section saturated early for $b = 0$ in comparison with $b = 1$ fm for $r > 1$ fm. The nonlinear corrections to the IP-Sat and IP Non-Sat models show that those behaviors are comparable in the range $0 \leq r \leq 4$ for the impact parameter $b = 1$ fm.

In conclusion, by considering the statistical errors due to the effective parameters, the nonlinear corrections to the dipole cross sections give a reasonable data description in comparison with the other models. Indeed, the GLR-MQ improved saturation model tames the DGLAP improved model behavior when the results compared to models described based on the recombination of gluons at low x .

Acknowledgements The author is grateful to Razi University for the financial support of this project.

Data Availability Statement This manuscript has no associated data or the data will not be deposited. [Authors' comment: We did not use experimental data directly. Rather, we have used models corresponding to the dipole cross sections.]

Open Access This article is licensed under a Creative Commons Attribution 4.0 International License, which permits use, sharing, adaptation, distribution and reproduction in any medium or format, as long as you give appropriate credit to the original author(s) and the source, provide a link to the Creative Commons licence, and indicate if changes were made. The images or other third party material in this article are included in the article's Creative Commons licence, unless indicated otherwise in a credit line to the material. If material is not included in the article's Creative Commons licence and your intended use is not permitted by statutory regulation or exceeds the permitted use, you will need to obtain permission directly from the copyright holder. To view a copy of this licence, visit <http://creativecommons.org/licenses/by/4.0/>.

Funded by SCOAP³. SCOAP³ supports the goals of the International Year of Basic Sciences for Sustainable Development.

References

1. K. Golec-Biernat, M. Wüsthoff, Phys. Rev. D **59**, 014017 (1999)
2. K. Golec-Biernat, S. Sapeta, JHEP **03**, 102 (2018)
3. J. Bartels, K. Golec-Biernat, H. Kowalski, Phys. Rev. D **66**, 014001 (2002)
4. B. Sambasivam, T. Toll, T. Ullrich, Phys. Lett. B **803**, 135277 (2020)
5. J.R. Forshaw, G. Shaw, JHEP **12**, 052 (2004)
6. E. Iancu, A. Leonidov, L. McLerran, Nucl. Phys. A **692**, 583 (2001)
7. E. Iancu, A. Leonidov, L. McLerran, Phys. Lett. B **510**, 133 (2001)
8. E. Iancu, K. Itakura, S. Munier, Phys. Lett. B **590**, 199 (2004)
9. Yu.L. Dokshitzer, Sov. Phys. JETP **46**, 641 (1977)
10. G. Altarelli, G. Parisi, Nucl. Phys. B **126**, 298 (1977)
11. V.N. Gribov, L.N. Lipatov, Sov. J. Nucl. Phys. **15**, 438 (1972)
12. A.H. Mueller, J. Qiu, Nucl. Phys. B **268**, 427 (1986)
13. L.V. Gribov, E.M. Levin, M.G. Ryskin, Phys. Rep. **100**, 1 (1983)
14. N.N. Nikolaev, W. Schäfer, Phys. Rev. D **74**, 014023 (2006)
15. N.N. Nikolaev, B.G. Zakharov, Z. Phys. C **49**, 607 (1991)
16. N.N. Nikolaev, B.G. Zakharov, Z. Phys. C **53**, 331 (1992)
17. W. Qinq-Dong et al., Chin. Phys. Lett. **33**, 012502 (2016)
18. H. Kowalski, D. Teaney, Phys. Rev. D **68**, 114005 (2003)
19. J.L. Abelleira Fernandez et al. [LHeC Study Group], J. Phys. G **39**, 075001 (2012)
20. P. Agostini et al. [LHeC Collaboration and FCC-he Study Group], J. Phys. G **48**, 110501 (2021)
21. A.H. Rezaeian, M. Siddikov, M. Van de Klundert, R. Venugopalan, Phys. Rev. D **87**, 034002 (2013)
22. A.H. Rezaeian, I. Schmidt, Phys. Rev. D **88**, 074016 (2013)
23. H. Kowalski, T. Lappi, R. Venugopalan, Phys. Rev. Lett. **100**, 022303 (2008)
24. H. Kowalski, T. Lappi, C. Marquet, R. Venugopalan, Phys. Rev. C **78**, 045201 (2008)
25. A.H. Mueller, Nucl. Phys. B **335**, 115 (1990)
26. L. McLerran, R. Venugopalan, Phys. Rev. D **49**, 2233 (1994)
27. J. Bartels, K. Golec-Biernat, H. Kowalski, Acta Phys. Polon. B **33**, 2853 (2002)
28. K. Golec-Biernat, S. Sapeta, Phys. Rev. D **74**, 054032 (2006)
29. G. Watt, H. Kowalski, Phys. Rev. D **78**, 014016 (2008)
30. V.S. Fadin, E.A. Kuraev, L.N. Lipatov, Phys. Lett. B **60**, 50 (1975)
31. L.N. Lipatov, Sov. J. Nucl. Phys. **23**, 338 (1976)
32. I.I. Balitsky, L.N. Lipatov, Sov. J. Nucl. Phys. **28**, 822 (1978)
33. K. Golec-Biernat, J. Phys. G **28**, 1057 (2002)
34. K. Golec-Biernat, Acta Phys. Polon. B **33**, 2771 (2002)
35. Y.S. Jeong, C.S. Kim, M.V. Luu, M.H. Reno, JHEP **11**, 025 (2014)
36. G.R. Boroun, Eur. Phys. J. C **82**, 740 (2022)
37. G.R. Boroun, Eur. Phys. J. Plus **137**, 371 (2022)
38. G.R. Boroun, B. Rezaei, Eur. Phys. J. C **81**, 851 (2021)
39. M.R. Pelicer et al., Eur. Phys. J. C **79**, 9 (2019)
40. M. Deveci, J.K. Sarma, Eur. Phys. J. C **74**, 2751 (2014)
41. E.L. Berger, M.M. Block, C.-I. Tan, Phys. Rev. Lett. **98**, 242001 (2007)
42. M.M. Block, L. Durand, D.W. McKay, Phys. Rev. D **77**, 094003 (2008)
43. M.M. Block, L. Durand, [arXiv:0902.0372](https://arxiv.org/abs/0902.0372) [hep-ph]
44. J. Kwiecinski et al., Phys. Rev. D **42**, 3645 (1990)
45. H. Abramowicz et al. (H1 and ZEUS Collaborations), Eur. Phys. J. C **78**, 473 (2018)